A feasible high spatiotemporal resolution breast DCE-MRI protocol for clinical settings

Luminita A. Tudorica[a, b, c, d, 1], Karen Y. Oh[a, 1], Nicole Roy[a], Mark D. Kettler[a],
Yiyi Chen[d, e], Stephanie L. Hemmingson[b], Aneela Afzal[b], John W. Grinstead[f],
Gerhard Laub[g], Xin Li[b], Wei Huang[b, d,*]

[a]Diagnostic Radiology, Oregon Health & Science University, Portland, OR, USA
[b]Advanced Imaging Research Center, Oregon Health & Science University, Portland, OR, USA
[c]Radiation Medicine, Oregon Health & Science University, Portland, OR, USA
[d]Knight Cancer Institute, Oregon Health & Science University, Portland, OR, USA
[e]Public Health and Preventive Medicine, Oregon Health & Science University, Portland, OR, USA
[f]Siemens Healthcare, Portland, OR, USA
[g]Siemens Healthcare, San Francisco, CA, USA

Abstract

Three dimensional bilateral imaging is the standard for most clinical breast dynamic contrast-enhanced (DCE) MRI protocols. Because of high spatial resolution (sRes) requirement, the typical 1–2 min temporal resolution (tRes) afforded by a conventional full-k-space-sampling gradient echo (GRE) sequence precludes meaningful and accurate pharmacokinetic analysis of DCE time-course data. The commercially available, GRE-based, k-space undersampling and data sharing TWIST (time-resolved angiography with stochastic trajectories) sequence was used in this study to perform DCE-MRI exams on thirty one patients (with 36 suspicious breast lesions) before their biopsies. The TWIST DCE-MRI was immediately followed by a single-frame conventional GRE acquisition. Blinded from each other, three radiologist readers assessed agreements in multiple lesion morphology categories between the last set of TWIST DCE images and the conventional GRE images. Fleiss' κ test was used to evaluate inter-reader agreement. The TWIST DCE time-course data were subjected to quantitative pharmacokinetic analyses. With a four-channel phased-array breast coil, the TWIST sequence produced DCE images with 20 s or less tRes and ~ $1.0\times1.0\times1.4$ mm^3 sRes. There were no significant differences in signal-to-noise (P=.45) and contrast-to-noise (P=.51) ratios between the TWIST and conventional GRE images. The agreements in morphology evaluations between the two image sets were excellent with the intra-reader agreement ranging from 79% for mass margin to 100% for mammographic density and the inter-reader κ value ranging from 0.54 (P<.0001) for lesion size to 1.00 (P<.0001) for background parenchymal enhancement. Quantitative analyses of the DCE time-course data provided higher breast cancer diagnostic accuracy (91% specificity at 100% sensitivity) than the current clinical practice of morphology and qualitative kinetics assessments. The TWIST sequence may be used in clinical settings to acquire high spatiotemporal resolution breast DCE-MRI images for both precise lesion morphology characterization and accurate pharmacokinetic analysis.
© 2012 Elsevier Inc. All rights reserved.

Keywords: Breast cancer; Dynamic contrast-enhanced (DCE) MRI; TWIST; Temporal resolution; Spatial resolution

1. Introduction

Magnetic resonance imaging (MRI) plays an important role in clinical care of breast patients. It is increasingly used for high-risk population screening, dense breast diagnosis, diagnostic problem solving, preoperative staging, therapy monitoring, and residual disease evaluation. Dynamic contrast-enhanced MRI (DCE-MRI) is a critical part of a

* Corresponding author. Advanced Imaging Research Center, Oregon Health & Science University, Portland, OR 97239 USA. Tel.: +1 503 418 1534; fax: +1 503 418 1543.
E-mail address: huangwe@ohsu.edu (W. Huang).
[1] equal contribution.

routine clinical breast MRI examination protocol. DCE-MRI images provide both tumor morphology and contrast kinetics information, which are decisive in image interpretation and follow-up recommendation by a radiologist. Tumor morphology assessment has been shown to play an important role in breast cancer diagnosis [1–3]. Post-contrast DCE-MRI images are often used for such purposes. Contrast kinetics features in a tumor are extracted from the DCE-MRI signal intensity time course.

Three-dimensional (3D) bilateral imaging is the standard for breast DCE-MRI protocols at most clinical sites. Typically, DCE images are acquired with a conventional gradient echo (GRE) pulse sequence, which employs full k-space sampling strategy. The trade-off between spatial and temporal resolution (sRes and tRes) in such an acquisition scheme and the radiologist's preference for high sRes in a clinical protocol result in a typical tRes of 1–2 min, even with the use of parallel imaging acceleration methods [4]. Consequently, the standard clinical approach to describe contrast kinetics from the DCE signal intensity time-course data is either qualitative evaluation of curve shapes [5] or semi-quantitative assessment of empirical quantities, such as signal enhancement ratio [6], maximum slope [7,8], washout ratio [9], *etc.*. However, the results from either approach are often dependent on the MRI scanner (magnetic field strength, vendor), data acquisition details (pulse sequence and parameters), contrast dose and/or injection rate, personnel skills, *etc.*, and these factors vary site-to-site. This contributes to limited specificity and lack of high reproducibility for breast DCE-MRI [10].

It has been shown that quantitative analysis of DCE-MRI time-course data, i.e., pharmacokinetic modeling to extract pharmacokinetic parameters, can potentially improve accuracy in breast cancer detection [11–15] and is valuable for monitoring therapeutic response to neoadjuvant chemotherapy [16–18]. Furthermore, one recent study [19] showed that the threshold value of a pharmacokinetic parameter for discrimination of benign and malignant breast lesions was largely independent of scanner platform, field strength, data acquisition parameters, and contrast agent selection. This is precisely one of the main reasons why DCE-MRI should be performed quantitatively. However, the 1–2 min tRes of most current clinical breast DCE-MRI protocols is inadequate for quantitative data analysis. High tRes is required for accurate and meaningful pharmacokinetic analysis [20]. By down-sampling the acquired DCE-MRI time-courses, a recent study [21] has demonstrated that as tRes decreases, the derived pharmacokinetic parameters K^{trans} and v_e are progressively under- and over-estimated, respectively. With regard to breast DCE-MRI, the results from simulations show that the cancer detection accuracy suffers if the tRes is degraded to the range of current clinical protocols, regardless of whether the quantitative [22] or semi-quantitative [23] data analysis approach is used. Therefore, in order for quantitative breast DCE-MRI to be adopted as a useful and practical imaging modality in clinical settings, it must be demonstrated that the

image data can be collected with high sRes and tRes simultaneously: the former for precise tumor morphology evaluation and the latter for accurate quantitative pharmacokinetic analysis.

To shorten acquisition time in 3D MRI, such as a breast DCE-MRI exam, one strategy is to abandon the approach of uniformly sampling the entire k-space at every time point. Random partial k-space updating [24] is a good example of such method and half k-space sampling like the HASTE sequence [25] is now routinely used in clinical MRI. However, these methods come at a cost of reduced signal-to-noise ratio (SNR). There have been significant research efforts in recent years to improve breast DCE-MRI tRes while preserving adequate SNR and sRes. Han *et al* [26] speeded up bilateral breast DCE-MRI by combining spiral imaging with TSENSE (adaptive sensitivity encoding incorporating temporal filtering) acceleration and achieved $1.1 \times 1.1 \times 3.0$ mm^3 sRes with a tRes of 11 s. Dougherty *et al* [27] combined SENSE parallel imaging [4] with a weighted radial view-sharing scheme – KWIC (k-space weighted image contrast) – to obtain an effective tRes of 15 s for $0.5 \times 0.5 \times 3.0$ mm^3 sRes. Several groups [28–30] have demonstrated up to 10x acceleration for DCE-MRI (without employing parallel imaging) by using the compressed sensing concept for image reconstruction [31], which allows filling of missing k-space data by constrained optimization. Simulations using k-spaced-fully-sampled breast DCE-MRI data have shown that the DCE signal time-course and derived pharmacokinetic parameters can be faithfully reproduced using the compressed sensing reconstruction method [28–30]. Though promising, the above mentioned techniques are not ready for implementation at clinical sites. In addition, the computation time for reconstruction of the usually large breast DCE-MRI image volume is demanding for the compressed sensing method [29,30]. For clinical practice, the impact of quantitative breast DCE-MRI would be immediate and significant if a commercially available pulse sequence were able to accomplish the goal of high spatiotemporal resolution. The solution may lie in the time-resolved MR angiography (MRA) sequences recently introduced by the major MR instrument manufacturers. These include General Electric's TRICKS (time resolved imaging of contrast kinetics) [32,33], Philips' 4D-TRAK (4D-time resolved MRA with keyhole) [34,35], and Siemens' TWIST (time-resolved angiography with stochastic trajectories) [36,37]. Generally using the keyhole imaging approach, these sequences have, while preserving SNR, readily addressed the sRes and tRes trade-off problem that is typical for conventional MRA.

The potential of the TRICKS sequence for high spatiotemporal resolution DCE-MRI has recently been evaluated with encouraging results [38,39]. In this study, we investigated the feasibility of using the GRE-based, 3D TWIST sequence for high sRes and tRes breast DCE-MRI in a pre-biopsy patient cohort with suspicious lesions. The SNR and CNR (contrast-to-noise ratio) of the TWIST images, as well as lesion morphology assessments, were compared to

those of the conventional GRE images with full k-space sampling. Quantitative analyses of the TWIST DCE time courses were performed for the purpose of differentiating benign and malignant lesions.

2. Materials and methods

2.1. The TWIST sequence

The TWIST pulse sequence is a GRE type sequence with 3D k-space data acquisition [36,37]. During a dynamic scan, it performs partial k-space undersampling, with emphasis on more frequent sampling of the k-space center, which governs image signal intensity and contrast, relative to the k-space periphery, which governs image fine detail. The TWIST sequence separates the k_y-k_z plane into two regions: an inner central region **A** and an outer peripheral region **B** (Fig. 1A). After an initial "Prep" phase of two seconds to bring the magnetization into steady state, the TWIST sequence acquires full k-space data only at the beginning (meas #1 in Fig. 1B). From here on, the **A** region is fully sampled in each repetition with A% defining the percentage of the data points in **A** relative to the total data points in the k_y-k_z plane, while the **B** region is sampled using a k-space trajectory with a reduced density with B% defining the percentage of the

sampled data points relative to the total data points in **B**. B% is equal to 1/3 in the example shown in Fig. 1B. All k-space points are sorted according to their radial distances from the k-space center, and the k-space orders in **A** and **B** are defined such that a spiral-like trajectory occurs with k-space distance going from the outer to the inner edge of the **B** region, and from the outer edge to the center in the **A** region, respectively. To reconstruct 3D image data for each measurement (or time frame) of a dynamic scan, the missing portions of the **B** region are copied from the neighboring B acquisitions, as shown in Fig. 1B. Assuming it takes time T_A and T_B to measure all k-space points in regions **A** and **B**, respectively, the tRes of a dynamic scan using a conventional GRE sequence is $T_A + T_B$. For a dynamic TWIST scan, with A% of all k-space points and only B% of the k-space points in the **B** region are acquired in each repetition, the effective tRes is $(T_A + T_B)[A\% + B\%(1 - A\%)]$. The smaller the A% and/or the B% values, the shorter the time interval between two consecutive measurements, leading to higher tRes. In addition, the TWIST sequence can be combined with parallel imaging techniques to further improve tRes.

2.2. Study population

This research study was approved by the Institutional Review Board and was Health Insurance Portability and
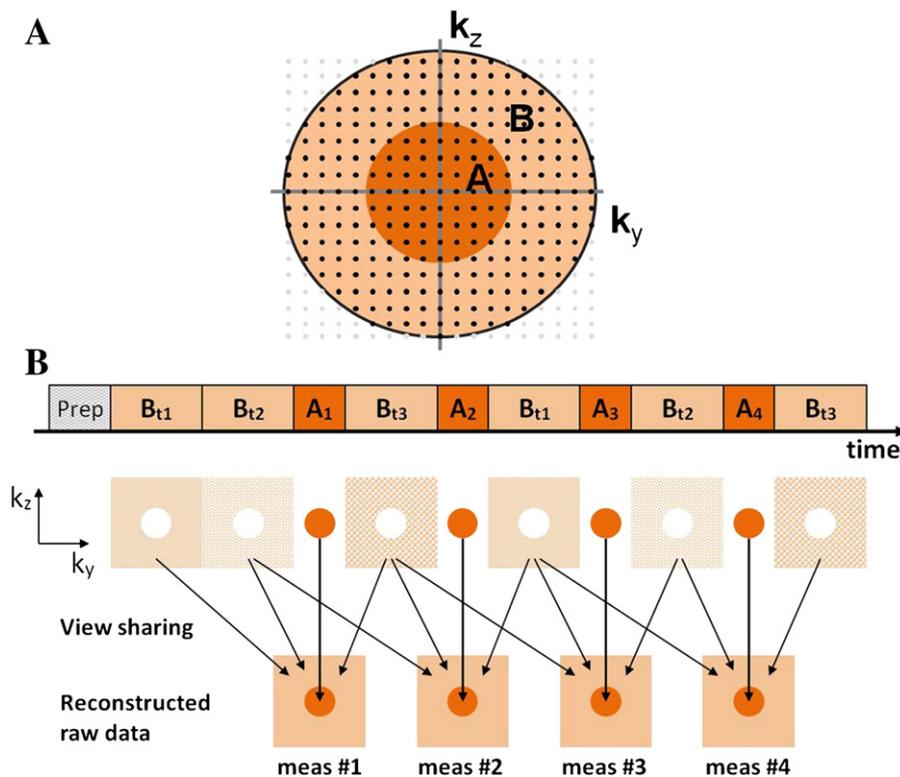

Fig. 1. **A.** The TWIST sequence 2D k-space coverage is displayed. Each dot represents a read-out line in the 3rd k-space dimension. The TWIST acquisition divides k-space into a center region **A** and a periphery region **B**. **B.** Example of a TWIST dynamic scan with B%=1/3. After a full k-space acquisition for the first measurement (meas #1), each following measurement acquires all of **A** and a pseudostochastically determined **B** portion. The missing portions of the **B** region are copied from the neighboring B acquisitions for image reconstruction. A_n: acquisition of k-space data points in region **A** for measurement #n; B_{t1}, B_{t2}, and B_{t3}: k-space trajectory 1, 2, and 3 in region **B** with equal portion of data points.

Accountability Act (HIPAA) compliant with written informed consent. The thirty-one enrolled subjects (mean age: 49 years, range: 32–85 years) are patients who had mammography- and/or sonography-detected suspicious lesions and were referred for stereotactic or ultrasound-guided core needle biopsies as standard care. A total of 36 suspicious lesions were detected in the 31 patients (three with 2 lesions each and one with 3 lesions), which were all rated in the BIRADS (Breast Imaging Reporting And Data System) 4 – suspicious – category. According to the clinical imaging interpretation reports, the mean tumor size (in the longest dimension) of this cohort was 13.4 mm, with a 3.0 – 32.0 mm range. Each enrolled subject underwent a research MRI session prior to the biopsy procedure.

2.3. MRI data acquisition

The MRI data acquisitions were conducted using a 3T MR system (Tim Trio; Siemens Healthcare, Erlangen, Germany) with a body transmit and four-channel phased-array bilateral breast receive RF coils. Following pilot scans and routine axial multi-slice T_2-weighted MRI (with fat saturation) and 3D T_1-weighted MRI (without fat saturation), axial bilateral breast DCE-MRI images with fat-saturation and full breast coverage were acquired with the TWIST sequence. Fat saturation in the TWIST acquisition was achieved with a 1-2-1 binomial water excitation pulse. For this study, the A% and B% values of the TWIST sequence were set at 0.15 and 0.2, respectively, corresponding to a 3.125-fold acceleration compared to a conventional GRE sequence. These numbers were selected based on findings from a recent kidney MRA study [37] that showed less than 5% errors in a TWIST DCE-MRI signal intensity time-course when A% and B% were both set at 0.2, compared to a full-k-space-sampling acquisition. Other acquisition parameters included 10° flip angle, 2.9/6.2 ms TE/TR, a parallel imaging acceleration factor of two, 30–34 cm FOV, 320x320 matrix size, and 120 or 128 slices with 1.4 mm slice thickness, resulting in $\sim 1.0 \times 1.0 \times 1.4$ mm^3 sRes. The acquisition times for the first TWIST DCE-MRI frame (full-k-space-sampling) were 57 s and 63 s, while those for the rest of the frames, the de facto DCE-MRI tRes, were 18 and 20 s for the 120-slice and 128-slice image volumes, respectively. The total DCE-MRI acquisition time was ~ 10 min. At the beginning of the third DCE-MRI frame acquisition, gadolinium-based contrast agent, ProHance (Bracco Diagnostics Inc., Princeton, NJ, USA), was administered intravenously (0.1 mmol/kg at 2 mL/s) through an antecubital vein by a programmable power injector, followed by 20 mL saline flush.

For pre-contrast T_1 determination - for the purpose of pharmacokinetic modeling of the DCE-MRI data, proton density-weighted images were collected immediately before DCE-MRI with the same acquisition setup except for 5° flip angle and 50 ms TR. For the purpose of TWIST *vs.* conventional GRE image comparison, a single-frame DCE-

MRI image volume was acquired immediately after the TWIST DCE-MRI scan with the same prescription of the TWIST acquisition (including the same parallel imaging acceleration factor), except that a conventional full-k-space-sampling 3D GRE sequence was used, resulting in a tRes of ~ 60 s.

2.4. SNR and CNR measurement and comparison

In the last TWIST DCE image set, a circular region of interest (ROI) was drawn in non-enhanced normal parenchyma area, a second ROI was placed within contrast-enhanced tumor region (except for tumor of focus type (< 5 mm)) in an image slice with the brightest contrast enhancement (in comparison to adjacent slices that also contained contrast-enhanced tumor areas) by visual inspection, and a third ROI was placed in the background noise (Fig. 2). All three ROIs had the same size (6 pixels), and were spatially registered to the conventional GRE images. The mean and standard deviation (SD) of the ROI signal intensities were recorded, and the SNR and CNR were calculated for both image sets for comparison purpose. The SNR was defined as

$$SNR = S_P / SD_N \tag{1}$$

where S_P was the mean signal intensity of the normal parenchyma ROI, and SD_N was the SD of the noise. The CNR was defined as

$$CNR = (S_T - S_P) / SD_N \tag{2}$$

where S_T was the mean signal intensity of the ROI in the contrast-enhanced tumor region.

2.5. MRI lesion morphology evaluation and comparison

All 36 mammography- and/or sonography-detected lesions exhibited MRI contrast enhancement. To determine whether tumor morphology characterization obtained from
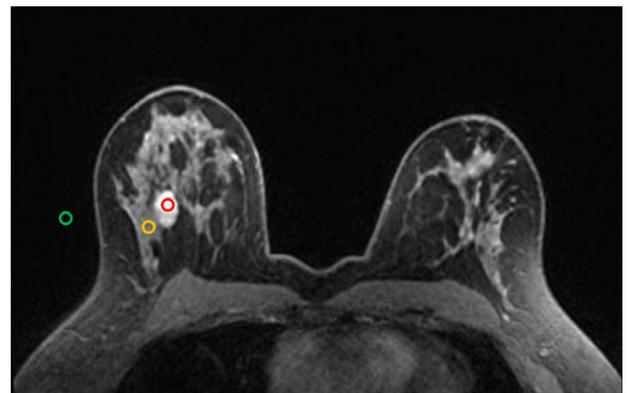

Fig. 2. An axial image from a last set of TWIST DCE-MRI images, showing a contrast-enhanced tumor in the right breast. Three circular ROIs of equal size (6 pixels) were placed in the tumor region (red), non-enhancing normal parenchyma region (yellow), and background noise (green) for image signal intensity measurements.

the TWIST DCE-MRI scan is equivalent to that from the conventional DCE-MRI scan, three experienced breast radiologists (KYO, NR, and MDK, each with at least five years experience in reading breast MRI) compared the last set of TWIST DCE-MRI images with the conventional full-k-space-sampling GRE images in multiple morphology categories based on the American College of Radiology (ACR) BIRADS MRI Lexicon [40], and gave "yes" or "no" decisions to indicate whether or not the morphology assessments agreed with each other. These categories included lesion enhancement type (focus, mass, or non-mass), shape (of mass), margin (of mass), internal enhancement pattern (of mass and non-mass), tissue mammographic density, background parenchymal enhancement, and lesion size. The exception is in the tissue mammographic density category, for which the radiologists rated "E" for "extremely dense", "H" for "heterogeneously dense", "S" for "scattered", and "F" for "fatty". The comparisons conducted by the three radiologists were blinded from each other.

2.6. Qualitative and quantitative analyses of TWIST DCE-MRI data

One pre- (the baseline image set acquired immediately before contrast injection) and five post-contrast image sets were selected from the TWIST DCE series to form a new dynamic series with a time interval (effective tRes) of 72 (120-slice image volume) or 80 (128-slice image volume) s between two consecutive image sets, essentially replicating the tRes and number of measurements of the institutional clinical DCE-MRI protocol using a conventional GRE sequence. These six image sets were submitted to a computer aided diagnosis (CAD) system (DynaCad, Invivo, Gainesville, FL, USA) for qualitative contrast kinetics evaluations. The three radiologist readers classified the DCE curve shapes as "washout", "plateau", and "persistent", and assigned BIRADS scores to the enhanced lesions based on both morphology and qualitative kinetics assessments [40]. In case of disagreement in morphology evaluation between the TWIST and conventional GRE images, the more suspicious evaluation was taken into account in determining the BIRADS score.

On an off-line computer workstation, the radiologists drew ROIs circumscribing the contrast-enhanced lesions. The lesion ROI and pixel (within the ROI) TWIST DCE time-course data were then subjected to the Standard Model (SM, or Tofts model) [41] and Shutter-Speed Model (SSM) [11,42,43] pharmacokinetic analyses – the latter accounts for intercompartmental water exchange kinetics. For the quantitative data analysis, pre-contrast T_1 values were calculated by comparing signal intensities between the proton density-weighted images and the baseline images from the DCE series [44]. A population-averaged arterial input function (AIF), which was determined from a previous breast DCE-MRI study with the same contrast injection protocol [11], was used in this study. The theory and mathematical formulations of the SM and SSM analyses have been previously described in great detail [41–43]. The lesion ROI pharmacokinetic parameter value was reported as the weighted (by ROI pixel numbers) average of that from each image slice where a contrast-enhanced lesion ROI was drawn.

2.7. Statistical analysis

Paired t test was used to determine if the SNR and CNR of the last TWIST DCE image set were significantly different from those of the conventional GRE image set. The proportion of agreement in morphology evaluations between the TWIST and the conventional GRE images was calculated for each radiologist reader and presented with the exact 95% confidence limits. The κ statistics was computed to assess inter-reader agreement among the three readers in morphology comparison, qualitative kinetics curve shape description, and MRI BIRADS score. κ statistics is a widely used measurement of inter-rater agreement for categorical data because it accounts for the agreement occurring by chance. κ=1 implies full agreement, while κ=0 implies agreement only by chance. The κ statistics reported here is the Fleiss' κ, the most commonly reported κ statistics for multiple raters [45]. Since the Fleiss' κ statistics does not incorporate the ordinal feature of mammographic density and BIRADS score, Kendall's coefficient of concordance was calculated for these two categories. The Kendall's coefficient of concordance is typically used in evaluating raters' agreement for ordered responses. It ranges from 0 (no agreement) to 1 (complete agreement). For all the variables of interest, a two-sized z test was used to evaluate whether the inter-reader agreement was significantly greater than by chance at a significance level of $P=.05$. All the statistical analyses were conducted using the SAS 9.2 software (SAS Institute Inc., Cary, NC, USA).

3. Results

3.1. SNR and CNR comparison

The SNR values in normal appearing, non-enhancing breast parenchyma were calculated for all 31 patients. The SNR measured from the last set of TWIST DCE images (mean±SD: 95±71) was not significantly ($P=.45$, paired t test) different from that measured from the conventional GRE images (104±64). The CNR values were calculated for 26 of the 36 lesions, because the other 10 lesions were focus type and too small for reliable tumor ROI signal intensity measurement. The CNR of the last set of TWIST DCE images (mean±SD: 58±39) was not significantly ($P=.51$, paired t test) different from that of the conventional GRE images (62±41).

3.2. Comparison of lesion morphology

The types of enhanced lesions were classified by the radiologists as focus, mass, and non-mass. Fig. 3 shows
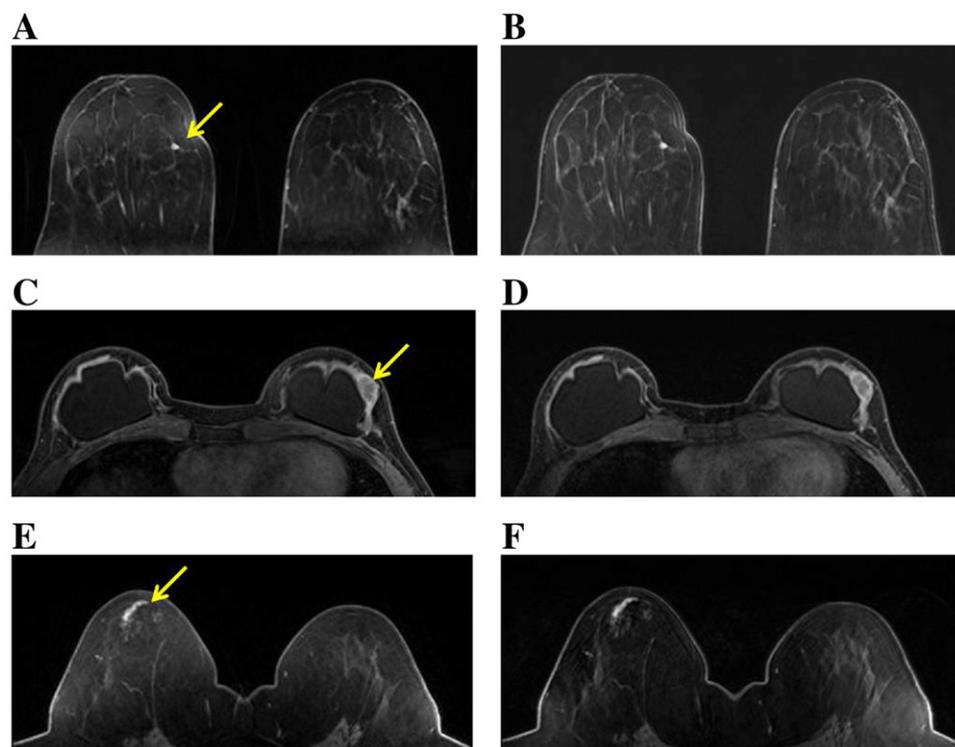
Fig. 3. Three pairs of post-contrast axial images from three women show three enhanced lesions (pointed by the arrows): a focus (A and B), a mass (C and D), and a non-mass (E and F). The images in the left column (A, C, and E) are from the last TWIST DCE-MRI image sets, while those in the right column (B, D, and F) are from the conventional GRE image sets. The two images in each pair had the same spatial location in the head-to-foot direction. For each woman, the TWIST DCE-MRI and the conventional GRE images were acquired with the same flip angle (10°), TE/TR (2.9/6.2 ms), FOV (34 cm for A and B; 32 cm for C and D, and E and F), in-plane matrix size (320×320), and slice thickness (1.4 mm).

examples of the same image slices from the last TWIST DCE image set and the conventional GRE image set, depicting the three lesion types. All three readers answered "yes" in type classifications of these three lesions when comparing the two image sets. The focus lesion (Fig. 3A and B) was pathologically proven to be a benign lesion with fibrocystic changes, while the mass (Fig. 3C and D) and non-mass (Fig. 3E and F) lesions were pathologically proven to be a malignant invasive ductal carcinoma and a malignant ductal carcinoma *in situ*, respectively.

The percentages of the lesions that had the same morphologic feature interpretations when comparing the two image sets are listed in Table 1 for each reader and each morphology category, as well as the Fleiss' κ values for inter-reader agreement. The intra-reader agreement in morphology between the two image sets ranged from 79% for mass margin to 100% for mammographic density. The κ value ranged from 0.54 ($P<.0001$) for lesion size to 1.00 ($P<.0001$) for background parenchymal enhancement. Besides κ=0.82 ($P<.0001$), Kendall's coefficient of concordance was 0.96 ($P<.0001$) for mammographic density evaluation.

The average MRI lesion size in the longest dimension was calculated for each lesion based on the three readers' measurements. The mean (13.8 mm) and range (3.6 – 32.0 mm) of the MRI lesion size were in excellent agreement with those of the mammographic/sonographic lesion size.

Table 1
Agreement in lesion morphology assessment between TWIST and conventional GRE images

	Type	Mass			Non-Mass	MD	BPE	Lesion Size
		Shape	Margin	IE	IE			
Reader 1	97% (85%, 100%)	96% (79%, 100%)	83% (63%, 95%)	96% (79%, 100%)	100%	100%	94% (81%, 99%)	94% (81%, 99%)
Reader 2	97% (85%, 100%)	96% (79%, 100%)	79% (58%, 93%)	96% (79%, 100%)	100%	100%	94% (81%, 99%)	92% (78%, 98%)
Reader 3	97% (85%, 100%)	96% (79%, 100%)	83% (63%, 95%)	92% (73%, 99%)	100%	100%	94% (81%, 99%)	89% (74%, 97%)
κ statistics	1.00 ($P<.0001$)	1.00 ($P<0.0001$)	0.72 ($P<0.0001$)	0.74 ($P<0.0001$)	1.00	0.82 ($P<.0001$)	1.00 ($P<0.0001$)	0.54 ($P<.0001$)

IE: internal enhancement; MD: mammographic density; BPE: background parenchymal enhancement.
The numbers in parentheses for each reader are 95% exact confidence limits. They were not calculated for the non-mass IE and MD categories because, when comparing the two image sets, each reader considered these two morphologic features equivalent for every lesion.
The P values were from z test. It was not calculated for non-mass IE category because there was not sufficient number of non-masses (2 in the 36-lesion cohort).

3.3. Comparison of diagnoses by clinical MRI protocol and quantitative DCE-MRI

The biopsy pathology analyses revealed that thirteen lesions were malignant and the other 23 lesions were benign (Table 2), resulting in a positive predictive value (PPV) for biopsy of 36% for the clinical mammographic/ sonographic diagnoses.

The readers had excellent agreement in qualitative contrast kinetics assessments using the CAD system, with κ=0.78 (P<.0001, z test). The lesion MRI BIRADS scores, based on the readers' interpretations of both morphology and qualitative kinetics, are given in Table 3. Again, the three readers had considerable agreements in giving BIRADS scores, with κ=0.87 (P<.0001, z test) and Kendall's coefficient of concordance equal 0.95 (P<.0001). None of the readers made a false negative diagnosis, attaining 100% diagnostic sensitivity each. Their diagnostic specificities and PPVs were in the ranges of 65-69% and 62-65%, respectively (Table 3).

Fig. 4 shows the ROI K^{trans}(SSM) (Fig. 4A) and ΔK^{trans} (Fig. 4B) scatter plots for the 36 lesions. ΔK^{trans}, which is defined as $\Delta K^{trans} \equiv K^{trans}$(SSM) - K^{trans}(SM), measures the effects of water exchange on K^{trans} estimation [11,42]. Using K^{trans}(SSM) as the diagnostic marker, a cut-off value of 0.08 min^{-1} (Fig. 4A) gave an improved specificity (compared to the radiologists' diagnoses) of 83% at 100% sensitivity. With the same cut-off value obtained from another patient cohort [42], 0.024 min^{-1} (Fig. 4B), the ΔK^{trans} marker provided an even higher specificity of 91% at 100% sensitivity. Fig. 4C and D demonstrate the ΔK^{trans} maps of a malignant invasive ductal carcinoma and a benign fibroadenoma, respectively. With the same color scale, the malignant lesion exhibited large areas of hot spots, while none was observed in the benign lesion. With 74% specificity and 100% sensitivity at a cut-off value of 0.05 min^{-1}, the diagnostic accuracy of the K^{trans}(SM) marker was not as good as the K^{trans}(SSM) and ΔK^{trans} markers. The sensitivity, specificity, and PPV values of the K^{trans}(SM), K^{trans}(SSM), and ΔK^{trans} parameters are listed in Table 3.

4. Discussion

It is gratifying to observe that the ROI ΔK^{trans} cut-off value which achieved 100% sensitivity and specificity in a cohort of mainly mammography-occult lesions [42] attained 91% specificity and 100% sensitivity in this study of a mammography-visible lesion population. These two DCE-MRI studies were conducted at different field strength and with different scanner platform, data acquisition details (pulse sequence and parameters), and gadolinium contrast agent. The fact that one single cut-off value performed similarly well in two different patient cohorts undergoing different DCE-MRI protocols demonstrates the essence of quantitative imaging – the imaging biomarkers are biological quantities, in principle independent of how imaging data

Table 2
Lesion pathologies (N=36)

Pathology	Number and Grade
Malignant [a]	
invasive ductal carcinoma	10 (3 grade III, 4 grade II, 3 grade I)
invasive lobular carcinoma	2 (1 grade I, 1 grade II)
ductal carcinoma *in situ*	1 (grade III)
Benign	
lobular carcinoma *in situ* [b]	1
atypical ductal hyperplasia [b]	2
benign parenchyma	5
fibroadenoma	5
fibrocystic changes	6
intraductal papilloma [b]	1
fibroadenomatous lesion	1
fibroepithelial lesion	1
sclerosing adenosis	1

[a] Core biopsy pathologies were confirmed by subsequent surgical biopsy pathologies.

[b] High risk benign lesions. Subsequent surgical biopsies of these high risk lesions as standard care found no malignancies.

are collected and processed. Furthermore, this study, together with other studies [11–15], shows that the approach of quantitative DCE-MRI improves diagnostic accuracy for breast cancer compared to the current standard approaches of clinical breast MRI. These are some of the main reasons why quantitative imaging is the future for clinical cancer imaging, whether for diagnosis or treatment planning and monitoring. Adaptation of quantitative DCE-MRI in a clinical breast MRI protocol implies the need for imaging speed acceleration while preserving high sRes, which is an essential requirement by radiologists for image interpretation.

The TWIST breast DCE-MRI protocol used in this study generated high sRes bilateral axial images with near isotropic 1 mm voxel size, which is well above the minimum requirement for sRes by the ACR for breast DCE-MRI [40]. The intra- and inter-radiologist reader agreements in comparisons of all categories of tumor morphologic features between the TWIST and the conventional full-k-space-sampling GRE images were excellent, indicating that it is feasible to achieve, without sacrificing sRes, high tRes for breast DCE-MRI with the TWIST sequence – 20 s or 18 s with the data acquisition schemes employed in this study. Though full k-space data were not acquired in TWIST DCE-MRI (except for the first time frame), the DCE images at each time frame were reconstructed with full k-space data [36,37]. Thus, not surprisingly, the SNR of the non-enhancing normal breast parenchyma in the last set of TWIST DCE images was not significantly different from that in the conventional GRE images. For lesion morphology comparisons, it would have been ideal if the extent of contrast enhancement had been the same for the two image sets. We fitted the tumor ROI signal intensities of the last six DCE time frames with a straight line and calculated its slope and angle relative to a horizontal line. The angles ranged from + 2.9° to −7.4° for the 36-lesion cohort. Thus, insignificant differences in the extent of contrast enhancement can be assumed between the last

Table 3
Breast cancer diagnostic accuracy: sensitivity, specificity, and PPV

	BIRADS 2	BIRADS 3	BIRADS 4	BIRADS 5	Sensitivity	Specificity	PPV
Reader 1	13	2	19	2	100%	65%	62%
Reader 2	12	3	20	1	100%	65%	62%
Reader 3	13	3	18	2	100%	69%	65%
K^{trans}(SM)	-	-	-	-	100%	74%	68%
K^{trans}(SSM)	-	-	-	-	100%	83%	76%
ΔK^{trans}	-	-	-	-	100%	91%	87%

BIRADS 2: benign; BIRADS 3: probably benign; BIRADS 4: suspicious abnormality; BIRADS 5: highly suggestive of malignancy. BIRADS 4 and 5 are positive diagnoses, resulting in biopsy recommendations. PPV: positive predictive value for biopsy. $\Delta K^{trans} \equiv K^{trans}$(SSM) $- K^{trans}$(SM).

TWIST DCE and conventional GRE images, i.e., there was no significant contrast agent wash-in or wash-out occurring in the tumor between the acquisitions of the two image sets. In addition, the fact that the CNR was not significantly different between the two image sets provides further evidence that this was the case (see Eq. [2]) and our approach of morphology comparison was valid.

The results from this study suggest that the use of the TWIST sequence, and possibly similar keyhole approach time-resolved MRA sequences from other major vendors, may provide a shortcut for rapid translation of quantitative breast DCE-MRI in clinical settings. The 20 s or shorter tRes achieved in this TWIST DCE-MRI study appears adequate for pharmacokinetic modeling of the time-course data and extracting the K^{trans} (and ΔK^{trans} when both the SM and SSM analyses are used) parameter that characterizes

malignant and benign breast lesions. Similar results were obtained from full-k-space-sampling breast DCE-MRI data with comparable tRes (albeit with much lower sRes and single breast coverage) [11,42]. When the intravascular compartment is included in the pharmacokinetic model to fit the data, the estimation of the additional parameter v_p, plasma volume fraction, is unlikely to be accurate at ~ 20 s tRes [43,46]. This is because the MRI signal contribution from the plasma occurs mainly during the early rising phase of the DCE time course, which can be accurately captured only with sufficient data sampling rate. Additionally, ~ 20 s tRes is not adequate for precise direct AIF measurement [20]. This problem can be resolved by using population averaged AIF determined from similar studies (using the same contrast injection protocol) with higher tRes, as is the case in this study, or using reference-region [47,48] or blinded estima-
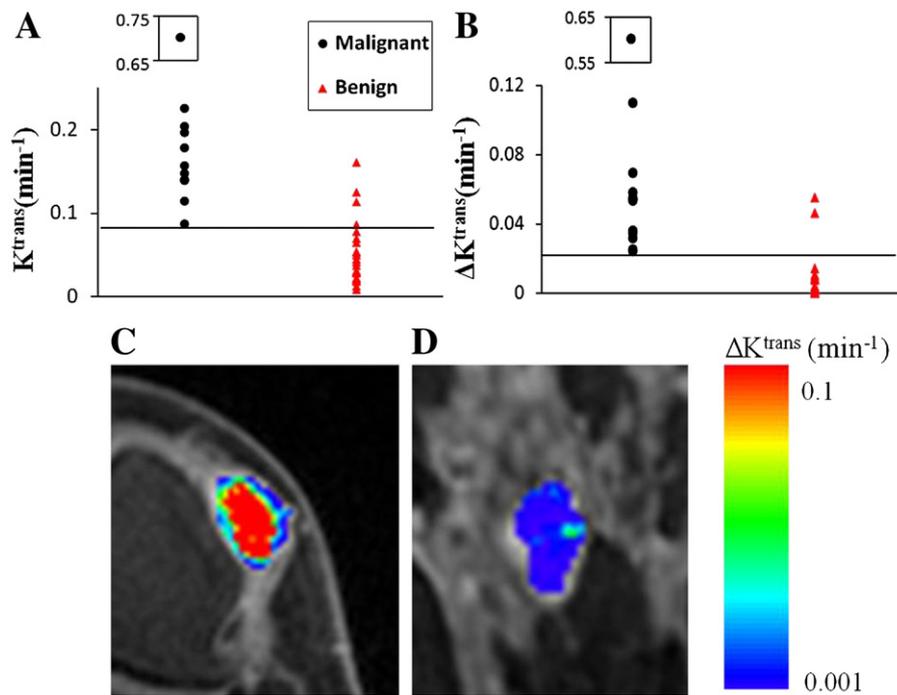

Fig. 4. Scatter plots of lesion ROI K^{trans}(SSM) (A) and ΔK^{trans} (B) values for thirteen malignant (black circles) and twenty three benign (red triangles) lesions. The insets show the outlier malignant lesion relative to the displayed scales. The horizontal lines represent 100% diagnostic sensitivity cut-off values of 0.08 min^{-1} (A) and 0.024 min^{-1} (B) for K^{trans}(SSM) and ΔK^{trans}, respectively. The latter was determined from another patient cohort with mainly mammography-occult lesions [42]. Zoomed pixel-by-pixel ΔK^{trans} color maps of a malignant invasive ductal carcinoma (C) and a benign fibroadenoma (D) are shown overlaid onto the corresponding post-contrast TWIST DCE-MRI images.

tion [49] methods. A four-channel phased-array receive coil and a parallel imaging acceleration factor of two were used in this study. With 16-channel phased-array breast coil currently commercially available and at least 3X faster parallel imaging acceleration (in comparison to a 4-channel coil) achievable, sub-10 s tRes for TWIST breast DCE-MRI, and therefore more accurate direct AIF measurement and v_p estimation, is feasible.

Unlike other sophisticated data acquisition methods [26,27] for improving breast DCE-MRI tRes, the TWIST sequence is commercially available and can be readily implemented in a clinical breast MRI protocol. Other commercially available, keyhole approach pulse sequences include the TRICKS and 4D-TRAK sequences. Though it has been shown that signal intensity time course from a TRICKS DCE-MRI acquisition closely matches that from a full-k-space-sampling acquisition [38], the effects of the TRICKS k-space undersampling strategy on tumor morphology assessment have not been evaluated. In comparison to the TRICKS sequence which uses linear trajectory when sampling one central and one of several periphery k-space sections, the TWIST sequence uses a spiral and pseudostochastic trajectory to traverse a full range of k-space with theoretical advantage in image quality and artifacts reduction [36]. For broader adoption of high spatiotemporal resolution breast DCE-MRI in clinical settings, it may be beneficial to investigate, as in this study, the feasibilities of using the TRICKS and 4D-TRAK sequences for breast DCE-MRI. Recently, the compressed sensing method for image reconstruction from undersampled k-space data has emerged to be a potentially ground-breaking technique for high speed imaging without sacrificing sRes. Through simulations using full-k-space-sampled data, several studies [28–30] demonstrated the potential of the compressed sensing method for high spatiotemporal resolution breast DCE-MRI. However, in these studies compressed sensing image reconstructions were performed at the same DCE time points as the actually acquired, low tRes full-k-space data. Even though the resulting, simulated signal intensity time courses have been shown to closely match those of the actually acquired data, whether compressed sensing reconstruction of an actually acquired, k-space-undersampled, high tRes DCE-MRI data set can closely reproduce the time course of a full-k-space data set is yet to be investigated. Moreover, the effects of this reconstruction method on tumor morphology characterization have not been evaluated. Another recent study [50] shows that the choice of k-space undersampling schemes can influence both quality and temporal fluctuation of the final DCE images reconstructed using the compressed sensing algorithm. Therefore, further investigations need to be conducted before compressed sensing can be used as a commercial product in clinical settings to perform high spatiotemporal resolution breast DCE-MRI.

Since the images at each time frame are reconstructed with full-k-space data, the signal intensity time course of a dynamic TWIST scan perfectly reproduces that of a full-k-space-sampling dynamic scan on static signals. However, for DCE-MRI studies with varying signal intensities due to contrast agent uptake and washout, the potential of the TWIST sequence for high sRes and tRes quantitative DCE-MRI can be fully realized only after its sampling strategy is optimized to maintain signal intensity time course and fine image details that are afforded by a conventional full-k-space-sampling GRE sequence. For TWIST DCE-MRI data acquisition in this study, the fraction of k-space region **A** and the reduced sampling density in region **B** were set at fixed values that have been shown in a MRA study [37] to incur minimal errors in signal intensity (< 5%). Optimization of the combined A% and B% values through simulations should be explored in future research to potentially further improve the tRes of TWIST breast DCE-MRI, while ensuring the reliability of signal intensity time course and minimizing image artifacts.

In conclusion, with appropriate k-space undersampling strategy, the TWIST sequence can be used in clinical settings to acquire breast DCE-MRI data with both high sRes and tRes: the former for precise tumor morphology assessment; the latter for accurate pharmacokinetic analysis of the time-course data.

Acknowledgments

References

[1] Goto M, Ito H, Akazawa K, Kubota T, Kizu O, Yamada K, et al. Diagnosis of breast tumors by contrast-enhanced MR imaging: comparison between the diagnostic performance of dynamic enhancement patterns and morphologic features. J Magn Reson Imaging 2007;25:104–12.

[2] Kuhl CK, Schild HH, Morakkabati N. Dynamic bilateral contrast-enhanced MR imaging of the breast: trade-off between spatial and temporal resolution. Radiology 2005;236:789–800.

[3] Schnall MD, Blume J, Bluemke DA, De Angelis GA, DeBruhl N, Harms S, et al. Diagnostic architectural and dynamic features at breast MR imaging: multicenter study. Radiology 2006;238:42–53.

[4] Friedman PD, Swaminathan SV, Smith R. SENSE imaging of the breast. AJR Am J Roentgenol 2005;184:448–51.

[5] Kuhl CK, Mielcareck P, Klaschik S, Leutner C, Wardelmann E, Gieseke J, et al. Dynamic breast MR imaging: are signal intensity time course data useful for differential diagnosis of enhancing lesions? Radiology 1999;211:101–10.

[6] Kaiser WA, Zeitler E. MR imaging of the breast: fast imaging sequences with and without Gd-DTPA. Preliminary observations. Radiology 1989;170:681–6.

[7] Moate PJ, Dougherty L, Schnall MD, Landis RJ, Boston RC. A modified logistic model to describe gadolinium kinetics in breast tumors. Magn Reson Imaging 2004;22:467–73.

[8] Buadu LD, Murakami J, Murayama S, Hashiguchi N, Sakai S, Masuda K, et al. Breast lesions: correlation of the contrast medium

enhancement patterns on MR images with histopathologic findings and tumor angiogenesis. Radiology 1996;200:639–49.

[9] Ikeda O, Yamashita Y, Morishita S, Kido T, Kitajima M, Okamura K, et al. Characterization of breast masses by dynamic enhanced MR imaging. A logistic regression analysis. Acta Radiol 1999;40:585–92.

[10] Jansen SA, Shimauchi A, Zak L, Fan X, Wood AM, Karczmar GS, et al. Kinetic curve of malignant lesions are not consistent across MRI systems: need for improved standardization of breast dynamic contrast-enhanced MRI acquisition. Am J Roentgen 2009;193:832–9.

[11] Huang W, Tudorica LA, Li X, Thakur SB, Chen Y, Morris EA, et al. Discrimination of benign and malignant breast lesions by using shutter-speed dynamic contrast-enhanced MR imaging. Radiology 2011;261:394–403.

[12] Schabel MC, Morrell GR, Oh KY, Walczak CA, Barlow RB, Neumayer LA. Pharmacokinetic mapping for lesion classification in dynamic breast MRI. J Magn Reson Imaging 2010;31:1371–8.

[13] Eyal E, Badikhi D, Furman-Haran E, Kelcz F, Kirshenbaum KJ, Degani H. Principal component analysis of breast DCE-MRI adjusted with a model-based method. J Magn Reson Imaging 2009;30:989–98.

[14] Vincensini D, Dedieu V, Eliat PA, Vincent C, Bailly C, de Certaines J, et al. Magnetic resonance imaging measurements of vascular permeability and extracellular volume fraction of breast tumors by dynamic Gd-DTPA-enhanced relaxometry. Magn Reson Imaging 2007;25:293–302.

[15] Brix G, Kiessling F, Lucht R, Darai S, Wasser K, Delorme S, et al. Microcirculation and microvasculature in breast tumors: pharmacokinetic analysis of dynamic MR image series. Magn Reson Med 2004;52:420–9.

[16] Ah-See MW, Makris A, Taylor NJ, Harrison M, Richman PI, Burcombe RJ, et al. Early changes in functional dynamic magnetic resonance imaging predict for pathologic response to neoadjuvant chemotherapy in primary breast cancer. Clin Cancer Res 2008;14:6580–9.

[17] Yankeelov TE, Lepage M, Chakravarthy A, Broome EE, Niermann KJ, Kelley MC, et al. Integration of quantitative DCE-MRI and ADC mapping to monitor treatment response in human breast cancer: initial results. Magn Reson Imaging 2007;25:1–13.

[18] Pickles MD, Lowry M, Menton DJ, Gibbs P, Turnbull LW. Role of dynamic contrast enhanced MRI in monitoring early response of locally advanced breast cancer to neoadjuvant chemotherapy. Breast Cancer Res Treat 2005;91:1–10.

[19] Springer CS, Tudorica LA, Li X, Thakur S, Morris EA, Oh KY, et al. Meta-population breast cancer screening with the ΔK^{trans} DCE-MRI parameter. Book of abstract: Nineteenth Annual Meeting of the International Society for Magnetic Resonance in Medicine. Berkeley (Calif): ISMRM; 2011. p. 3097.

[20] Henderson E, Rutt BK, Lee TY. Temporal sampling requirements for the tracer kinetics modeling of breast disease. Magn Reson Imaging 1998;16:1057–73.

[21] Heisen M, Fan X, Buurman J, van Riel NAW, Karczmar GS, ter Haar Romeny BM. The influence of temporal resolution in determining pharmacokinetic parameters from DCE-MRI data. Magn Reson Med 2010;63:811–6.

[22] Tagge IJ, Li X, Tudorica LA, Chen Y, Hemmingson S, Morris EA, et al. Effects of temporal resolution on breast cancer diagnostic accuracy by quantitative dynamic contrast-enhanced MRI. Book of abstract: Eighteenth Annual Meeting of the International Society for Magnetic Resonance in Medicine. Berkeley (Calif): ISMRM; 2010. p. 4748.

[23] El Khouli RH, Macura KJ, Barker PB, Habba MR, Jacobs MA, Bluemke DA. Relationship of temporal resolution to diagnostic performance for dynamic contrast enhanced MRI of the breast. J Magn Reson Imaging 2009;30:999–1004.

[24] Parrish T, Hu X. Continuous update with random encoding (CURE): a new strategy for dynamic imaging. Magn Reson Med 1995;33:326–36.

[25] Semelka RC, Kelekis NL, Thomasson D, Brown MA, Laub GA. HASTE MR imaging: description of technique and preliminary results in the abdomen. J Magn Reson Imaging 1996;6:698–9.

[26] Han M, Daniel BL, Hargreaves BA. Accelerated bilateral dynamic contrast-enhanced 3D spiral breast MRI using TSENSE. J Magn Reson Imaging 2008;28:1425–34.

[27] Dougherty L, Isaac G, Rosen MA, Nunes LW, Moate PJ, Bostan RC, et al. High frame-rate simultaneous bilateral breast DCE-MRI. Magn Reson Med 2007;57:220–5.

[28] Smith DS, Welch EB, Li X, Arlinghaus LR, Loveless ME, Koyama T, et al. Quantitative effects of using compressed sensing in dynamic contrast enhanced MRI. Phys Med Biol 2011;56:4933–46.

[29] Wang H, Miao Y, Zhou K, Yu Y, Bao S, He Q, et al. Feasibility of high temporal resolution breast DCE-MRI using compressed sensing theory. Med Phys 2010;37:4971–81.

[30] Chen L, Schabel MC, DiBella EVR. Reconstruction of dynamic contrast enhanced magnetic resonance imaging of the breast with temporal constraints. Magn Reson Imaging 2010;28:637–45.

[31] Lustig M, Donoho D, Pauly JM. Sparse MRI: the application of compressed sensing for rapid MR imaging. Magn Reson Med 2007;58:1182–95.

[32] Petkova M, Gauvrit JY, Trystram D, Nataf F, Godon-Hardy S, Munier T, et al. Three-dimensional dynamic time-resolved contrast-enhanced MRA using parallel imaging and a variable rate k-space sampling strategy in intracranial arteriovenous malformations. J Magn Reson Imaging 2009;29:7–12.

[33] Kunishima K, Mori H, Itoh D, Aoki S, Kabasawa H, Koga T, et al. Assessment of arteriovenous malformations with 3-Tesla time-resolved, contrast-enhanced, three-dimensional magnetic resonance angiography. J Neurosrug 2009;110:492–9.

[34] Willinek WA, Hadizadeh DR, von Falkenhausen M, Urbach H, Hoogeveen R, Schild HH, et al. 4D time-resolved MR angiography with keyhole (4D-TRAK): more than 60 times accelerated MRA using a combination of CENTRA, keyhole, and SENSE at 3.0T. J Magn Reson Imaging 2008;27:1455–60.

[35] Parmar H, Ivancevic MK, Dudek N, Gandhi D, Mukherji SK. Dynamic MRA with four-dimensional time-resolved angiography using keyhole at 3 tesla in head and neck vascular lesions. J Neuroophthalmol 2009;29:119–27.

[36] Lim RP, Shapiro M, Wang EY, Law M, Babb JS, Rueff LE, et al. 3D time-resolved MR angiography (MRA) of the carotid arteries with time-resolved imaging with stochastic trajectories: comparison with 3D contrast-enhanced bolus-chase MRA and 3D time-of-flight MRA. Am J Neuroradiol 2008;29:1847–54.

[37] Song T, Laine AF, Chen Q, Rusinek H, Bokacheva L, Lim RP, et al. Optimal k-space sampling for dynamic contrast-enhanced MRI with an application to MR renography. Magn Reson Med 2009;61:1242–8.

[38] Kershaw LE, Cheng HLM. A general dual-bolus approach for quantitative DCE-MRI. Magn Reson Imaging 2011;29:160–6.

[39] Ramsay E, Causer P, Hill K, Plewes D. Adaptive bilateral breast MRI using projection reconstruction time-resolved imaging of contrast kinetics. J Magn Reson Imaging 2006;24:617–24.

[40] American College of Radiology (ACR). Breast Imaging Reporting and Data System (BI-RADS), 4th ed; 2003.

[41] Tofts PS, Brix G, Buckley DL, Evelhoch JL, Henderson E, Knopp MV, et al. Estimating kinetic parameters from dynamic contrast-enhanced T1-weighted MRI of a diffusable tracer: standardized quantities and symbols. J Magn Reson Imaging 1999;10:223–32.

[42] Huang W, Li X, Morris EA, Tudorica LA, Seshan VE, Rooney WD, et al. The magnetic resonance shutter speed discriminates vascular properties of malignant and benign breast tumors *in vivo*. Proc Natl Acad Sci 2008;105:17943–8.

[43] Li X, Huang W, Morris EA, Tudorica LA, Seshan VE, Rooney WD, et al. Dynamic NMR effects in breast cancer dynamic-contrast-enhanced MRI. Proc Natl Acad Sci 2008;105:17937–42.

[44] Huang W, Wang Y, Panicek DM, Schwartz LH, Koutcher JA. Feasibility of using limited-population-based average R_{10} for

pharmacokinetic modeling of osteosarcoma dynamic contrast-enhanced MRI data. Magn Reson Imaging 2009;27:852–8.

[45] Fleiss JL. Statistical methods for rates and proportions. 2nd Ed. New York: Wiley; 1981.

[46] Sourbron SP, Buckley DL. On the scope and interpretation of the Tofts models for DCE-MRI. Magn Reson Med 2011;66:735–45.

[47] Yankeelov TE, Luci JJ, Lepage M, Li R, Debusk L, Lin PC, et al. Quantitative pharmacokinetic analysis of DCE-MRI data without an arterial input function: a reference region model. Magn Reson Imaging 2005;23:519–29.

[48] Yang C, Karczmar GS, Medved M, Stadler WM. Multiple reference tissue method for contrast agent arterial input function estimation. Magn Reson Med 2007;58:1266–75.

[49] Fluckiger JU, Schabel MC, DiBella EVR. Model-based blind estimation of kinetic parameters in dynamic contrast enhanced (DCE)-MRI. Magn Reson Med 2009;62:1477–86.

[50] Chan RW, Ramsay EA, Cheung EY, Plewes DB. The influence of radial sampling schemes on compressed sensing reconstruction in breast MRI. Magn Reson Med 2012;67:363–77.